J. Iron Steel Res. Int. (2018) 25:426–432
https://doi.org/10.1007/s42243-018-0039-x

ORIGINAL PAPER

Effect of two-step cooling process on mechanical properties of TRIP steel with high performance

M.L. Li[1,2] · H. Jiang[1,2] · Y.L. He[1,2] · L.B. Chen[1,2] · G.T. Zhang[3] · H. Wang[1] · X.G. Lu[1,2] · L. Li[1,2]

Received: 20 March 2017 / Revised: 8 October 2017 / Accepted: 10 October 2017 / Published online: 7 May 2018

Abstract
A novel two-step cooling experiment was established to simulate the slow cooling process of continuous annealing production line for transformation-induced plasticity (TRIP) steel. The microstructures and mechanical properties of TRIP steel soaked at 700 °C for different time were investigated by tensile test, scanning electron microscopy, X-ray diffraction, and thermodynamic and kinetic calculation. It is shown that the steel soaked for 15 s exhibits the optimal product of strength and elongation (PSE > 30,000 MPa%) due to the transformation of austenite to proeutectoid ferrite, which delays the bainite transformation and improves the stability of retained austenite. In addition, the mechanical properties of TRIP steel soaked over 30 s are much lower, resulting from the precipitation of cementite, which decreases the stability of retained austenite and weakens the TRIP effect.

Keywords Transformation-induced plasticity steel · Two-step cooling · Microstructure · Mechanical property

1 Introduction

As one of the solutions for lightweight automobile industry, low-alloyed cold-rolled transformation-induced plasticity (TRIP) [1] steels which are nominated by excellent combinations of high ultimate tensile strength (UTS), good total elongation (TE) and low costs have been developing very fast in recent years. Although 1100 MPa grade TRIP steels have already been investigated in the laboratory [2, 3], the production information of TRIP steels with about 30,000 MPa% PSE (product of strength and elongation) is quite little. As well known, continuous annealing production line is used to produce TRIP steel [4]. A slow cooling region between the heating units and cooling units of continuous annealing production line [5, 6] is different from the conventional TRIP treatments in the laboratory. The effect of austenite transformation during the slow cooling process on mechanical properties of TRIP steel is not clear yet.

In the present work, a two-step cooling experiment was established to simulate the continuous annealing production line of TRIP steel. The microstructures and mechanical properties of TRIP steel under different two-step cooling conditions were investigated by tensile test, scanning electron microscopy (SEM), transmission electron microscopy (TEM), X-ray diffraction (XRD), and thermodynamic and kinetic calculation, which provide theoretical knowledge for developing new-generation advanced high-strength steels.

2 Experimental material and procedure

The chemical composition of the investigated steel is shown in Table 1. A 150 kg ingot is produced in a vacuum induction furnace, hot-rolled to 3.5 mm and subsequently cold-rolled to 1.4 mm.

The investigated steel was annealed in a salt bath furnace, and the heat-treatment processes are shown in Fig. 1. Considering the condition of continuous annealing production line, the second soaking temperature of two-step

✉ Y.L. He
ylhe@t.shu.edu.cn

[1] School of Materials Science and Engineering, Shanghai University, Shanghai 200072, China

[2] State Key Laboratory of Advanced Special Steel, Shanghai University, Shanghai 200072, China

[3] Pangang Group Research Institute, Panzhihua 617000, Sichuan, China

Table 1 Chemical composition of investigated steel (wt%)

Element	C	Mn	Si	Al	V	Fe
Content	0.31	0.91	2.06	0.76	0.094	Balance

cooling treatment was set as 700 °C and the soaking time was set as 0, 15, 30 and 60 s respectively, marked sample 1, 2, 3, 4. Moreover, such heat treatments were repeated three times and then the results were averaged.

Mechanical properties were evaluated by conducting tensile tests at room temperature with crosshead speed of 2 mm/min on A50 specimens. XRD measurements were performed in a D/max-2550 X-ray diffractometer with Cu-Kα radiation. Scanning was carried out with a 0.02° stepping and allowing 3 s for each step over a 2θ range from 40° to 100°. The volume fraction of retained austenite (RA) under different heat-treatment conditions is calculated by Eq. (1) [7].

$$V_\gamma = \frac{1.4I_\gamma}{I_\alpha + 1.4I_\gamma} \tag{1}$$

where V_γ is the volume fraction of RA, %; I_γ is the average integrated intensity of diffraction peaks of $(220)_\gamma$ and $(331)_\gamma$; and I_α is the integrated intensity of diffraction peak of $(211)_\alpha$.

And then, the carbon content of RA is calculated by Eq. (2) [7].

$$C_\gamma = \frac{\alpha_\gamma - 3.578}{0.033} \tag{2}$$

where α_γ is the lattice constant of RA; and C_γ is the mass fraction of carbon contents of RA, %.

In addition, carbide particles were chemically extracted in phosphoric acid (2:1) at room temperature and filtered using a micro-porous membrane with 20 nm aperture and dried. A D/MAX-2500 X-ray diffractometer operating at 40 kV and 40 mA was used to determine the type of precipitates. The technique of carbon extraction replica was also used to investigate the carbide particles under the TEM observation. Carbon replica specimens were ground and polished, and then chemically etched with 4 vol.% nital. A carbon coating was deposited onto the etched surface. This film was then scored with sharp blade to divide it into several smaller squares of 9 mm^2. 8 vol.% nital was used to remove the carbon film, which then was washed in methanol and floated off in distilled water. The replicas were collected by a copper net. Precipitates were identified by a combination of electron diffraction patterns and energy-dispersive spectroscopy (EDS) analysis.

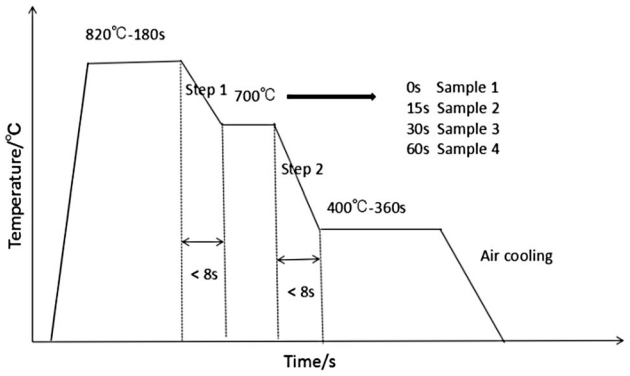

Fig. 1 Schematic diagram of two-step cooling heat-treatment processes

3 Results

As shown in Fig. 2, the microstructure of the investigated steel is composed of ferrite (F), bainite (B), and retained austenite (RA). XRD and TEM analyses of precipitations in the investigated steel with soaking time of 0 and 15 s are shown in Figs. 3 and 4, respectively. It can be seen that VC particles with size of a few nanometers exist in both samples. Thus, all samples' microstructures are composed of ferrite (F), bainite (B), retained austenite (RA) and VC particles. Besides, small VC particles, and some Fe_3C carbides exist in samples soaked for 30 and 60 s, as shown in Fig. 5a, b.

The mechanical properties of the samples under different two-step cooling heat-treatment conditions are shown in Table 2. The experimental results have good reproducibility, and the average values of UTS, TE and PSE of samples are presented in Fig. 6. It is shown that the sequence of PSE for the samples from the highest to lowest is the samples 2, 1, 3, 4 on the whole. Among them, the sample 2 exhibits the optimal PSE value which is greater than 30,000 MPa%.

4 Discussion

The kinetic model for calculating transformation of austenite was firstly presented by Kirkaldy [8]. The modified formula is given in Eq. (3) [9].

$$\tau_{\mathrm{TTT}} = \frac{1}{2^{\frac{N}{8}}(\Delta T)^3} \mathrm{e}^{\left(\frac{Q_{\mathrm{eff}}}{RT}\right)} \sum_{j=1}^{m} \alpha_j C_j \tag{3}$$

where τ_{TTT} is the transformation time; N is the number of ASTM grain size; ΔT is the undercooling degree of austenite, K; Q_{eff} is the effective diffusion rate; α_j is the empirical constant of each element; and C_j is the concentration of each element; R is the gas constant; and T is the temperature, K.

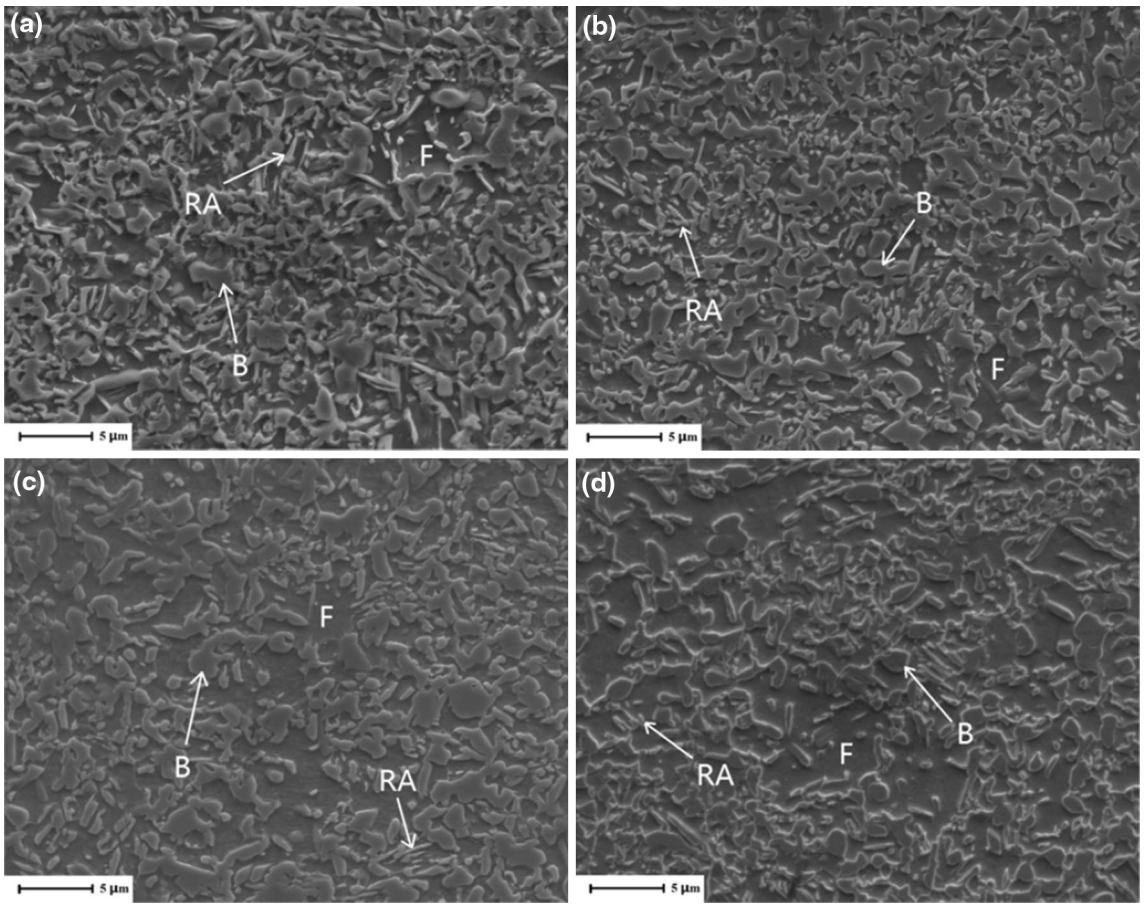

Fig. 2 SEM microstructures of investigated steels with different soaking time. **a** 0 s; **b** 15 s; **c** 30 s; **d** 60 s

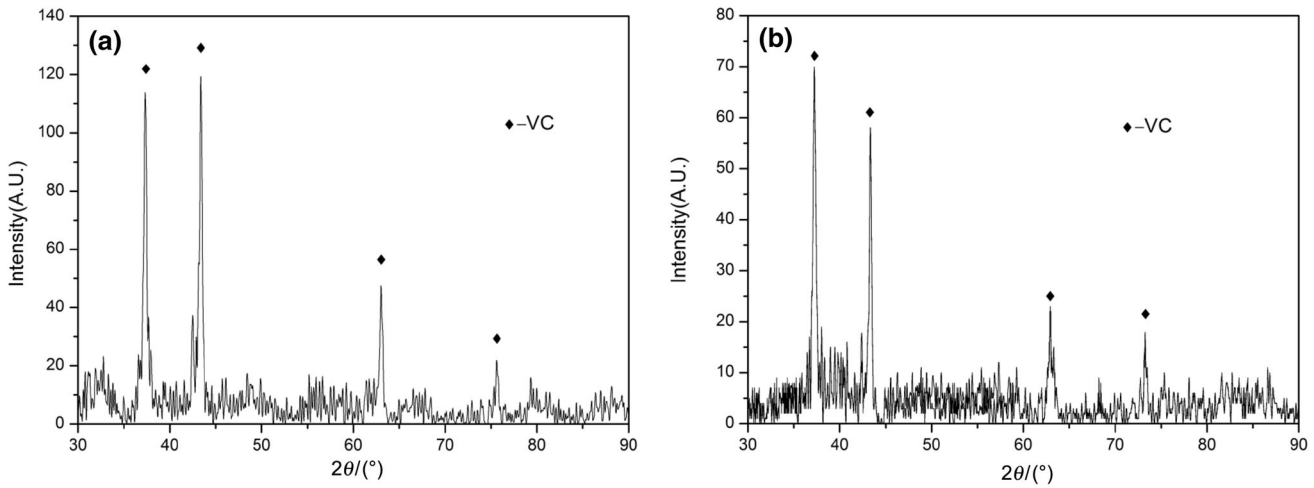

Fig. 3 XRD analysis of precipitations in investigated steel with soaking time of 0 s (**a**) and 15 s (**b**)

The grain size of austenite was measured by quantitative metallography method. In order to get a clear image of grain boundary, samples were etched by picric acid reagent, as shown in Fig. 7. The mean intercept of austenite grain is 3.26 μm, which can be transferred to $N = 13$.

Then, elements contents, i.e., C_j, in austenite of the investigated steel at intercritical annealing temperature of 820 °C are calculated by Thermo-Calc software, as shown in Table 3. While the other parameters are all given by JMatPro Software [9].

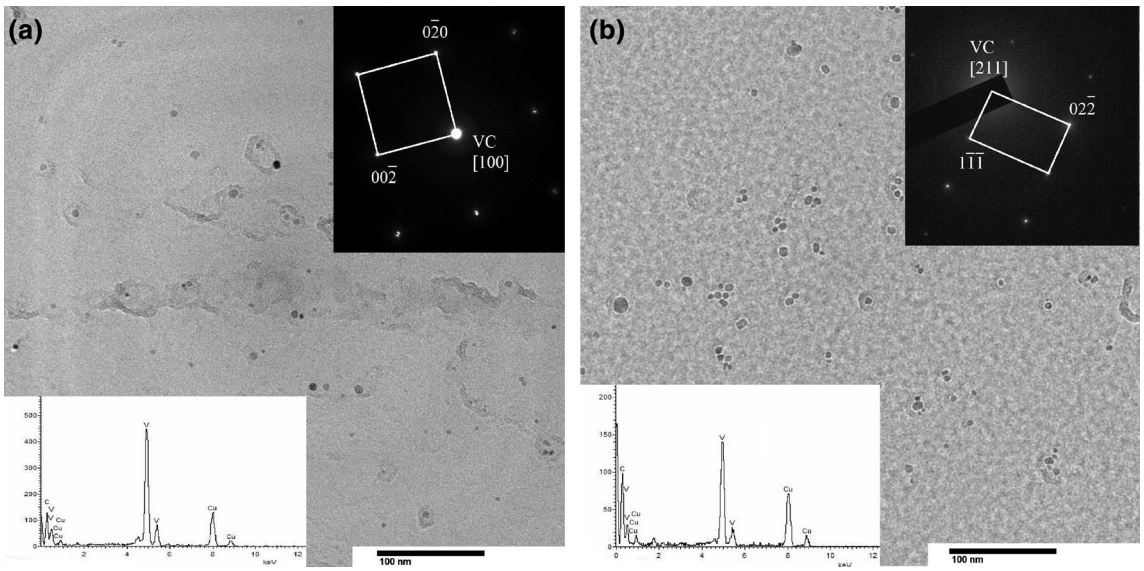

Fig. 4 TEM analysis of precipitations in investigated steel with soaking time of 0 s (**a**) and 15 s (**b**)

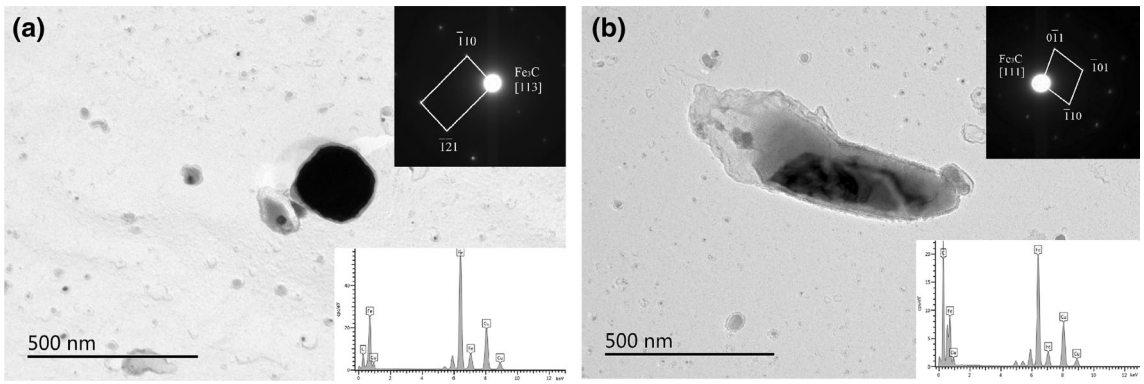

Fig. 5 TEM analysis of precipitations in investigated steel with soaking time of 30 s (**a**) and 60 s (**b**)

Table 2 Mechanical properties of the samples under different heat-treatment conditions

Sample	Cooling speed/(°C s^{-1})			Average UTS/MPa	Average TE/%
	Conventional heat treatment	Step 1	Step 2		
1	> 35			1038	28.8
2		> 15	> 35	1063	29.3
3		> 15	> 35	1025	24.2
4		> 15	> 35	1019	20.1

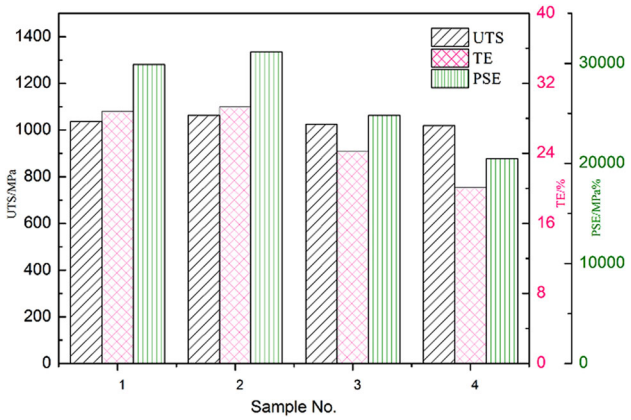

Fig. 6 Comparison of mechanical properties for samples under different heat-treatment conditions

The transformation of austenite in investigated steel is shown in Fig. 8. It can be seen that the formation temperature of pearlite is about 700 °C, which is in agreement with the results of thermodynamic calculation, as shown in Fig. 9. In addition, with the increase of soaking time at 700 °C, the transformation from austenite to proeutectoid ferrite happens between 4 s and 30 s, and the formation of pearlite can be observed after 30 s.

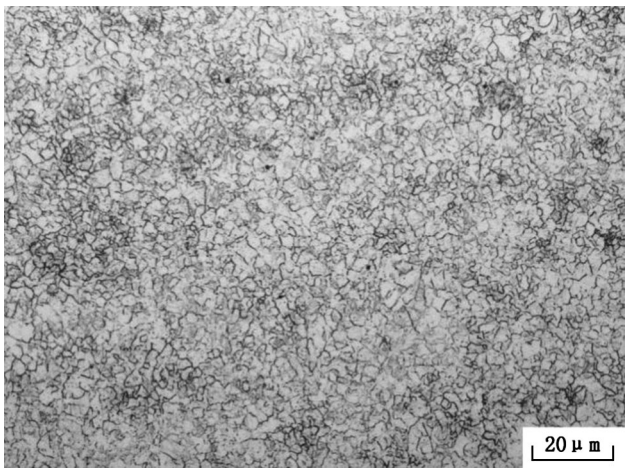

Fig. 7 Grain boundary image of austenite at 820 °C

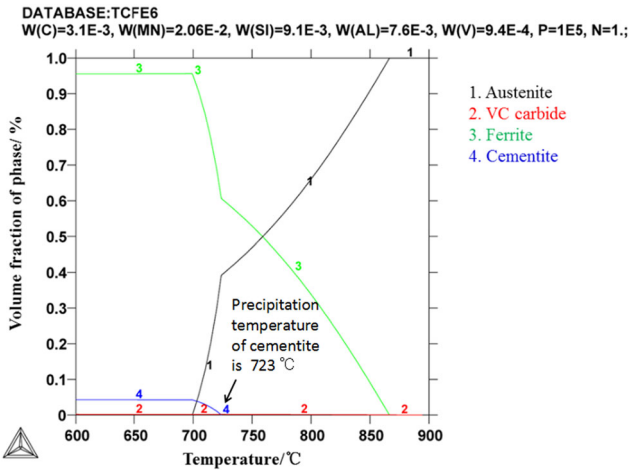

Fig. 9 Volume fraction of phases in investigated steel as a function of temperature

Table 3 Calculated elements contents in austenite at 820 °C (wt%)

Element	C	Mn	Si	Al	V	Fe
Content	0.39	2.38	0.89	0.66	0.029	Balance

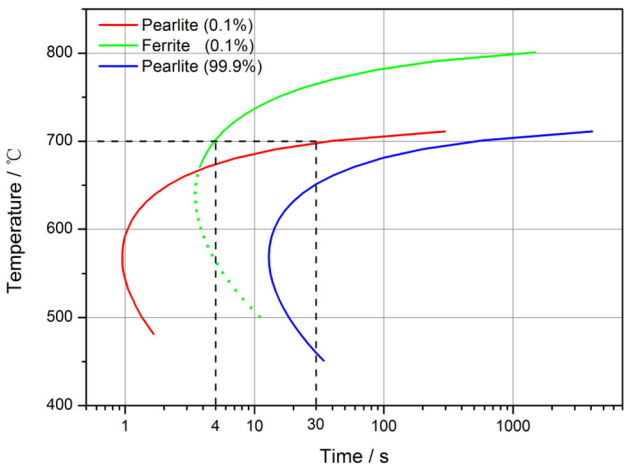

Fig. 8 Calculation results of transformation of austenite in investigated steels

According to Fig. 8, it can be concluded that the pearlite, composed of ferrite and cementite, formed in investigated steel at 700 °C after soaking for 30 s. The calculated results are in good agreement with the experimental results, as shown in Figs. 3, 4 and 5.

Combined with Fig. 6 and Table 2, sample 2 heated at 700 °C soaked for 15 s exhibits the optimal mechanical properties among all investigated samples. Compared with sample 1, the carbon content of austenite in sample 2 increases due to the transformation of austenite to proeutectoid ferrite, the bainite transformation is delayed during continuous cooling [10], and the stability of retained austenite is enhanced, resulting in good TRIP effect and improving the mechanical properties of the sample 2 which can reach 31,146 MPa%.

However, in samples 3 and 4, which were heated at 700 °C and soaked for 30 s and 60 s, respectively, the formation of pearlite is obviously observed. Thus, the retained austenite is not stable enough because of its lower carbon content, resulting in more and more precipitation of cementite. The weak TRIP effect deteriorates the mechanical properties, resulting in extremely low PSE for sample 4.

The volume fraction of retained austenite in investigated steel is further analyzed using XRD. As shown in Table 4, the volume fraction of retained austenite and the content of carbon in RA for sample 2 are the highest among the samples. It is well known that the mechanical properties of TRIP steel are mainly dependent on the stability of retained austenite [11–13]. A parameter S is introduced to evaluate the stability of retained austenite [14], $S = V_{RA} \cdot W_{RA}$, where V_{RA} is the volume fraction of retained austenite and W_{RA} is the mass fraction of carbon in retained austenite. It is obvious that the stability of retained austenite of sample 2 with the highest S value is optimal, resulting in the highest PSE.

Table 4 XRD results of RA of samples with different soaking time

Sample No.	Soaking time/s	Volume fraction of RA/%	Mass fraction of carbon in RA/%	S/%
1	–	19.49	1.08	0.211
2	15	21.09	1.13	0.238
3	30	17.01	1.00	0.170
4	60	16.40	0.99	0.162

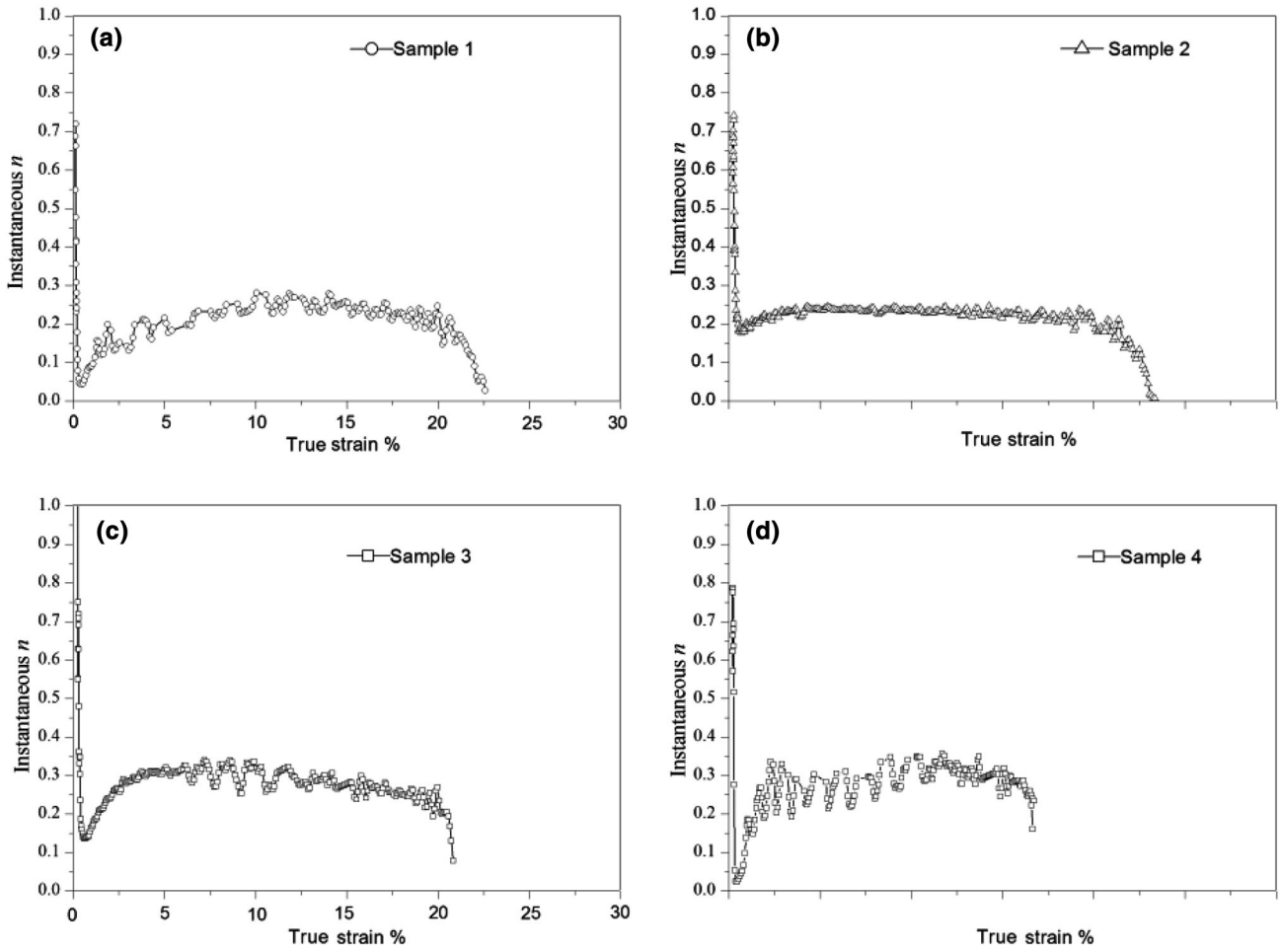

Fig. 10 Variation of instantaneous n value with true strain for samples with different soaking time. **a** 0 s; **b** 15 s; **c** 30 s; **d** 60 s

In order to obtain the detailed knowledge about the deformation mechanism of investigated steel, the instantaneous strain hardening exponents (n values) of samples with different soaking time are analyzed, as shown in Fig. 10. During the uniaxial tensile test, stress and strain follow the Hollomon equation, $\varepsilon = K \cdot \sigma^n$, where ε is the true strain, σ is the true stress, K is the strength coefficient, and n can be defined in Eq. (4) [15, 16]:

$$n_i = \frac{\partial(\ln\sigma)}{\partial(\ln\varepsilon)} \tag{4}$$

It can be seen that all the n values of investigated steel increase with increasing the strain at the beginning of deformation. The possible reasons are that large multiplication of dislocations makes the dislocation sliding difficult and the ferrite substrate strengthened [17]. Then, the n values of all samples will reach a certain value and keep stable for a long time, which is caused by the TRIP effect, that is phase transformation hardening and stress relaxation softening coexisted in matrix during the gradual transformation of retained austenite to martensite [18, 19]. Compared with the n values of samples 1 and 2, those of samples 3 and 4 decrease rapidly with increasing the strain. The possible reasons are that the carbon content of retained austenite and the stability of retained austenite; then the instantaneous transformation of martensite happens in the early stage of deformation, and thus, the effect of TRIP is obviously weakened.

5 Conclusion

A novel two-step cooling experiment was established to simulate the slow cooling process of continuous annealing production line for the TRIP steel. Combining experimental analysis with thermodynamic and kinetic calculation results, the microstructures and mechanical properties of the TRIP steel soaking at 700 °C for different time were investigated. It is shown that the steel with soaking time of 15 s exhibits the optimal product of strength and elongation (PSE > 30,000 MPa%) due to the transformation of austenite to proeutectoid ferrite, which delays the bainite

transformation and improves the stability of retained austenite. In addition, the mechanical properties of the TRIP steel soaking for over 30 s are much lower resulting from the precipitation of cementite, which weakens the TRIP effect and decreases the mechanical properties of the TRIP steel.

Acknowledgements This work was supported by National Key R&D Program of China (Grant No. 2017YFB0304402) and the Shanghai Municipal Natural Science Foundation (Grant No. 17ZR1410400).

References

[1] V.F. Zackay, E.R. Parker, D. Fahr, R. Busch, Trans. ASM 60 (1967) 250–259.
[2] H.X. Yin, Z.Z. Zhao, A.M. Zhao, X. Li, H.J. Hu, J.T. Liang, J. Iron Steel Res. Int. 22 (2015) 622–629.
[3] N.Q. Zhu, Study and Calculation of the Precipitation Behavior of Carbides in Automotive Steel and the Microstructure and Properties. Shanghai University, Shanghai, 2013.
[4] Y.B. Xu, X.Y. Hou, Y.Q. Wang, D. Wu, Acta Metall. Sin. 48 (2012) 176–182 (in Chinese).
[5] L.G. Gu, W.Z. Xu, Iron Steel Technol. 5 (2007) 13–15.
[6] Y.L. Kang, S. Guang, R.D. Liu, L. Yan, Angang Technol. 4 (2008) 1–8.
[7] D.J. Dyson, B. Holmes, J. Iron Steel Inst. 208 (1970) 469–474.
[8] J.S. Kirkaldy, Metall. Trans. 4 (1973) 2327–2333.
[9] N. Saunders, Z. Guo, X. Li, A.P. Miodownik, J.P. Schillé, The calculation of TTT and CCT diagrams for general steels, JMatPro Software Literature, 2004.
[10] L. Zhu, W. Di, X. Zhao, J. Iron Steel Res. Int. 15 (2008) No. 6, 68–71.
[11] S. Zhang, K.O. Findley, Acta Mater. 61 (2013) 1895–1903.
[12] L. Samek, E. De Moor, J. Penning, B.C. De Cooman, Metall. Trans. 37 (2006) 109.
[13] F. Hajiakbari, M. Nili-Ahmadabadi, B. Poorganji, T. Furuhara, Acta Mater. 58 (2010) 3073.
[14] J.B. Peng, L.B. Chen, H. Jiang, Y.L. He, L. Li, Transactions of Materials and Heat Treatment 37 (2016) 50–55.
[15] J. Chiang, B. Lawrence, J.D. Boyd, A.K. Pikey, Mater. Sci. Eng. A 528 (2011) 4516–4521.
[16] K. Sugimoto, N. Usui, M. Kobayashi, S. Hashimoto, ISIJ Int. 32 (1992) 1311–1318.
[17] Z.H. Cai, H. Ding, D.K. Misra, Z.Y. Ying, Acta Mater. 84 (2015) 229–236.
[18] S. Lee, S.J. Lee, B.C. De Cooman, Acta Mater. 59 (2011) 7546–7553.
[19] J.B. Peng, H. Jiang, G.T. Zhang, L.B. Chen, N.Q. Zhu, Y.L. He, X.G. Lu, L. Li, J. Iron Steel Res. Int. 24 (2017) 313–320.